Mesoscale fluvial erosion parameters deduced from modeling the Mediterranean sea level drop during the Messinian (late Miocene)

Nicolas Loget, Philippe Davy, Jean van den Driessche

Mesoscale fluvial erosion parameters deduced from modeling the Mediterranean sea level drop during the Messinian (late Miocene)

N. Loget,[1] P. Davy,[1] and J. Van Den Driessche[1]

Received 4 August 2005; revised 13 March 2006; accepted 21 April 2006; published 5 August 2006.

[1] After a base level drop, rivers are the first components of the landscape to respond by incising into topography. A base level drop results in a knickpoint in the downstream part of river longitudinal profiles. Whether knickpoints are preserved or erased during the upstream propagation of incision is still debated. Preservation and erasure of knickpoints are two end-member processes that work in natural systems at different timescales, different length scales, and different places. The huge (1500 m) and fast (tens of kiloyears) sea level drop in the Mediterranean during the Messinian resulted in the fast propagation of incision far inland. This is especially the case in the Rhone Valley (southern France) where the knickpoint is 300 km from the Mediterranean coast. Numerical modeling of this event has been performed using the €ros model, which simulates both erosional and depositional processes in rivers. The best fit between numerical results and geological data is obtained for a nonlinear relation between incision and drainage area and for a small transport length of sediment. This small transport length, at least 2 orders of magnitude lower than the length of the Rhone, suggests that the longitudinal profile relaxed in a diffusive way, so that the initial knickpoint was not preserved. Finally, after a base level fall, the propagation of fluvial incision is very fast at geological timescales (hundreds of kiloyears). Despite this, the diffusive response implies that the time required for restoration of an equilibrium profile is very long.

Citation: Loget, N., P. Davy, and J. Van Den Driessche (2006), Mesoscale fluvial erosion parameters deduced from modeling the Mediterranean sea level drop during the Messinian (late Miocene), *J. Geophys. Res.*, *111*, F03005, doi:10.1029/2005JF000387.

1. Introduction

[2] Numerous models have attempted to further the understanding of erosion processes at continental scales, especially with regards to hillslope and fluvial erosion [e.g., *Chase*, 1992; *Willgoose et al.*, 1991; *Kooi and Beaumont*, 1994; *Crave and Davy*, 2001; *Tucker and Slingerland*, 1996; *Braun and Sambridge*, 1997]. At that scale, the parameterization of erosion and deposition laws is necessarily lumped into some very crude parameters chosen for both their physical relevance, accessibility, and the expected model resolution. The crudest ''mean-field'' model describes the history of the mean topographic elevation; it has been parameterized by a constant erosion timescale in its simplest version [*Pinet and Souriau*, 1988]. Most of the current landscape evolution models are more sophisticated, and consider a spatially variable erosion pattern divided into two main spatial entities: hillslopes and a fluvial system represented by a network of 1D structures [e. g. *Howard et al.*, 1994; *Whipple and Tucker*, 1999]. In this model framework, there is quite a large consensus that the erosion and deposition laws depend on two main parameters: the local topographic slope and the drainage area, taken as a proxy for water discharge. However, the nature of the constitutive erosion laws is still an unresolved issue, with important consequences for the understanding of the physical geomorphological processes that prevail at such large length and timescales, on the predictions that can be made on landscape dynamics, and on the coupling between erosion, tectonic and climate.

[3] The parameters of these landscape evolution models can be constrained both by some theoretical considerations on the physics of erosion and sediment transport, and by natural examples for which the erosion can be quantified and fitted with models. We aim to develop the latter approach in this paper, by studying one of the most striking geological examples of erosional dynamics: the Messinian sea level drop and its consequences for the carving of a huge canyon along the Rhone Valley in France. The analysis of the canyon incision will be carried out within the framework of the landscape evolution models described above (with 1D rivers).

[4] The particular exercise of fitting net erosion patterns with erosion models has already been achieved by some recent studies. The main difficulty is the quantification of erosion, with a spatial resolution fine enough to make this inverse problem relevant. *Snyder et al.* [2000] and *Lague and Davy* [2003] used tectonic uplift as a reasonable estimate of erosion rates in areas where erosion and tectonic uplift are supposed to be at equilibrium. With this assumption, a morphometric measure such as the slope-area rela-

[1]Géosciences Rennes, UMR 6118, Centre National de la Recherche Scientifique, Université de Rennes 1, Rennes, France.

0148-0227/06/2005JF000387

tionship can be related to model parameters. There is, however, a fundamental indetermination in this approach since various erosion equations can fit the same data [e.g., *Whipple and Tucker*, 2002]. Transport-limited and detachment-limited models (see below) are both known to fit the observed power law relationship between slope and drainage area. The only way to solve this indetermination is to study transient topographic evolution [*Whipple and Tucker*, 1999; *Tucker and Whipple*, 2002; *Whipple and Tucker*, 2002]. *Stock and Montgomery* [1999], *van der Beek and Bishop* [2003], and *Tomkin et al.* [2003] have made use of well-dated erosion surfaces to deduce the amount of erosion in some river profiles. This approach is potentially richer than the analysis of steady state because the disequilibrium history contains the very nature of the erosion-transport equation. The main limitation is in the quality of the data set. These cited studies calculated the amount of erosion along a river profile as the difference between terraces (taken as a paleoriver profile) and the contemporary river. The amount of erosion is generally small compared to the height difference along the river profile, making the signal-to-noise ratio quite small. Some recent detailed studies eventually led to the frustrating conclusion that river profiles can be fitted by a variety of models with similar accuracy [*van der Beek and Bishop*, 2003] or by none of the existing incision models [*Tomkin et al.*, 2003], which illustrates the difficulty of dealing with small erosion amplitudes.

[5] Here we investigate an outstanding example of a huge sea level drop that occurred in the Mediterranean during the late Miocene. The closure of the marine gateways between Atlantic and Mediterranean waters resulted in the rapid desiccation of the Mediterranean Sea, inducing a 1500 m sea level drop and the carving of deep canyons along the preexisting drainage network. This event is called the Messinian salinity crisis (MSC) because desiccation was accompanied by the deposition of 1600 to 3200 m thick evaporites [*Hsü et al.*, 1973]. The MSC lasted about 600 kyr [e.g., *Krijgsman et al.*, 1999] and ended with the extremely rapid reflooding of the desiccated basin during the early Pliocene [*Blanc*, 2002], allowing rejuvenated relief all around the Mediterranean region to be "frozen" by Pliocene marine sedimentation [e.g., *Chumakov*, 1973; *Clauzon*, 1982; *Clauzon et al.*, 1996].

[6] The Messinian erosion history can be viewed as the ultimate experiment of bedrock incision. We aim to model the evolution of the profile of the Rhone River in order to derive the erosion transport parameters. We use a surface process model (∈ros), which introduces a transport length parameter that encompasses both detachment-limited and transport-limited equations into one single formulation. In the following, we first describe the ∈ros model, then we present the geological data and the modeling approach. From our results, we finally discuss the insights that the MSC example provides into the question of how large scale fluvial incision propagates.

2. ∈ROS Model

[7] We briefly present the principles used in the landscape evolution model ∈ros. The main characteristic of this model is that it is a particle method where equivalent raindrops (called precipitons) are launched on top of an erodible grid. A preliminary version of the code has been published in [*Davy and Crave*, 2000; *Crave and Davy*, 2001]. In such models, the physics of the modeled phenomena are embodied in a series of rules that specify how the running droplets interact with the topographic grid. With simple interaction rules, it is possible to create complex auto-organized spatial patterns with statistical properties similar to natural landforms [e.g., *Chase*, 1992; *Murray and Paola*, 1997].

[8] In ∈ros, each precipiton moves on top of the grid as water flows on top of the topography. It has a finite water volume but a variable discharge q that reflects changes in water velocity, depth or width. The method of calculating water discharge according to the precipiton distribution is given by *Crave and Davy* [2001].

[9] Precipitons transport the sediment load S and exchange mass with the topography h according to erosion-deposition rules. The consequent erosion and deposition fluxes depend on both water discharge, topographic gradients, and material erodibility. In contrast with other models [*Chase*, 1992], erosion flux is qualitatively different from deposition flux. The former is given by a surrogate of the classical stream power law relationship:

$$\dot{e} = K q_w^m s^n \tag{1}$$

where $\dot{e}$ is the erosion rate, q_w the river discharge, s the largest descending topographic slope, K a proxy for erodibility, and m and n two power law exponents. The deposition flux $\dot{d}$ is taken proportional to the sediment load S transported by the river/precipiton:

$$\dot{d} = \frac{S}{\tau} \tag{2}$$

where τ is a time constant, which quantifies the time spent by a particle within the river. Note that, if $\dot{d}$ is a deposition rate, S is the sediment load expressed as the equivalent thickness of sediment within the river. In ∈ros, the mass balance is calculated as the variation with distance of the sediment load carried by precipiton. In a Lagrangian reference frame that moves with the precipitons, the mass balance becomes:

$$dS = \left(\frac{\dot{e}}{v}dx - \frac{S}{\xi}dx\right), \tag{3}$$

where ξ is a transfer distance equal to the product of τ by the horizontal water velocity v. ξ is a basic parameter that has been used in some landscape evolution models [*Beaumont et al.*, 1992; *Kooi and Beaumont*, 1994]. It represents the typical distance that a river particle runs before depositing. It is also the typical distance for the sediment load to reach its equilibrium value if $\dot{e}$ is constant:

$$S_{eq} = \tau\dot{e} = \frac{\xi}{v}\dot{e} \tag{4}$$

The model is thus very close, if not similar, to the stream capacity concept where the net erosion/deposition flux is obtained by comparing the actual sediment load to its

theoretical capacity. Indeed, the net mass balance for topography is given by:

$$\frac{\partial h}{\partial t} = -\dot{e} + \dot{d} = -\dot{e} + \frac{S}{\tau} = \frac{(S_{eq} - S)}{\tau} \quad (5)$$

If ξ is small (compared to the grid size for instance), the topographic mass balance can be expressed as (see Appendix A for more details):

$$\frac{\partial h}{\partial t} = -\nabla(\xi \dot{e}) \quad (6)$$

If ξ is large, sediment never redeposits and the topographic mass balance contains only the erosion term (see Appendix A for more details):

$$\frac{\partial h}{\partial t} = -\dot{e} \quad (7)$$

[10] This formulation encompasses the two end-members of river incision model, i. e. detachment-limited and transport-limited models, so this kind of landscape evolution model is usually called a hybrid model [e.g., *Whipple and Tucker*, 2002]. Indeed if ξ is very small, the model simplifies to the transport-limited case whereas if ξ is very large, rivers carry all the eroded sediment out, as it is assumed in the detachment-limited case. In this paper, we consider ξ to be the tuning parameter that allows us to explore the range of possible models from detachment-limited to transport-limited. This approach offers the advantage of not presupposing the behavior of paleorivers.

[11] Note that ξ is also a physical parameter, which depends on the flow velocity, on the river depth, on the distribution of sediment in the river column, and on the downward grain velocity in the river flow. It is thus a function of both water discharge and sediment grain size via the vertical velocity term. The finest sediment grains tend to be transported very far from their locus of erosion, which means very large values of ξ; in contrast, large sediment grains are moving both episodically and close to the river bed, implying small transfer length values.

[12] Finally, we mention a specific problem that is general for this kind of landscape evolution model: the river width issue. For rivers considered as 1D structures, erosion transport equations such as (1) and (2) (or (4) or (5)) are normally integrated over the grid cell. If h is the average cell height, including both the river and its surroundings, the left-hand term is multiplied by the grid cell width dx. Since erosion is considered to be localized along the river, the right-hand term is integrated over the river width W leading to (note that we neglect some potential in-pixel sinuosity):

$$dx^* dh = W^*(-\dot{e} + \dot{d})dt \quad (8)$$

There is thus a ratio W/dx that appears in the mass balance equation. The problem here is that we have no complete information on the width of the valley or the river, so that it is not possible to calculate the average cell height. If now we consider the river profile height h_R rather than the average pixel height, the right-hand term is now integrated over river width only and the mass balance equation now writes:

$$W^* dh_R = W^*(-\dot{e} + \dot{d})dt \quad (9)$$

Since W appears on both the left and right sides of the equations, it disappears and equation (3) is also valid at the pixel scale. Note that this difference between pixel and river heights has already been mentioned in the formulation of some models [e.g., *Howard*, 1994; *Tucker et al.*, 2001; *Willett et al.*, 2001], and that it is implicit in studies that aim at analyzing river profiles [e.g., *Whipple and Tucker*, 1999; *Whipple*, 2001; *van der Beek and Bishop*, 2003]. This formulation implicitly assumes that the contribution of the off-river part of pixels is negligible; this is more than likely the case for the canyon incision of the Messinian story.

3. Messinian Sea Level Drop

[13] During Messinian times, a dramatic sea level fall took place in the Mediterranean, resulting from the closure of the gateways between the Atlantic and Mediterranean [e.g., *Weijermars*, 1988; *Martín et al.*, 2001]. This event is known as the Messinian salinity crisis (MSC) [e.g., *Hsü et al.*, 1973]. The base level drop is estimated to be 1500 m [*Ryan*, 1976] (Figures 1 and 2). Such an amplitude is comparable to that of base level variations induced by tectonic uplift, and is at least 1 order of magnitude higher than that induced by glacio-eustasy.

[14] Following this sea level drop, the pre-MSC drainage network was strongly incised by regressive erosion all around the Mediterranean region (Figures 1 and 2). Many Messinian canyons have been documented that underlie current valleys such as in the Nile, Rhone and Var Valleys [*Chumakov*, 1973; *Barber*, 1981; *Clauzon*, 1978, 1982]. Owing to catastrophic reflooding during the early Pliocene, these canyons have been preserved by Pliocene marine infilling deposits [*Denizot*, 1952; *Chumakov*, 1973]. Incision is very deep in the downstream part of these canyons (more than 1000 m for the Rhone and Nile) and has propagated very far inland (several 100 s km) (Figure 3). The corresponding incision rate is considerable, up to 10 mm yr^{-1} in the downstream part of the Rhone. This rate is similar to fluvial incision rates in tectonically active mountain belts as the Himalayas 2–12 mm yr^{-1} [e.g., *Burbank et al.*, 1996].

4. Geological Data

[15] In this study, we focus on the Messinian Rhone Valley (Figures 3 and 4). The Rhone Valley dates to the late Miocene [*Mandier*, 1988] and mainly developed between the French Alps to the east and the French Massif Central to the west (Figure 3). The current Rhone is about 800 km long and its drainage basin has an area of 100,000 km^2. During the MSC, incision propagated more than 300 km inland [*Clauzon*, 1982]. Numerous pre-Messinian tributary valleys were also reincised [e.g., *Ballesio*, 1972; *Mandier*, 1988; *Clauzon et al.*, 1995]. The Messinian Rhone Valley is one of the best documented Messinian canyons, both onshore and offshore, with numerous boreholes and seismic data (Figure 3), allowing

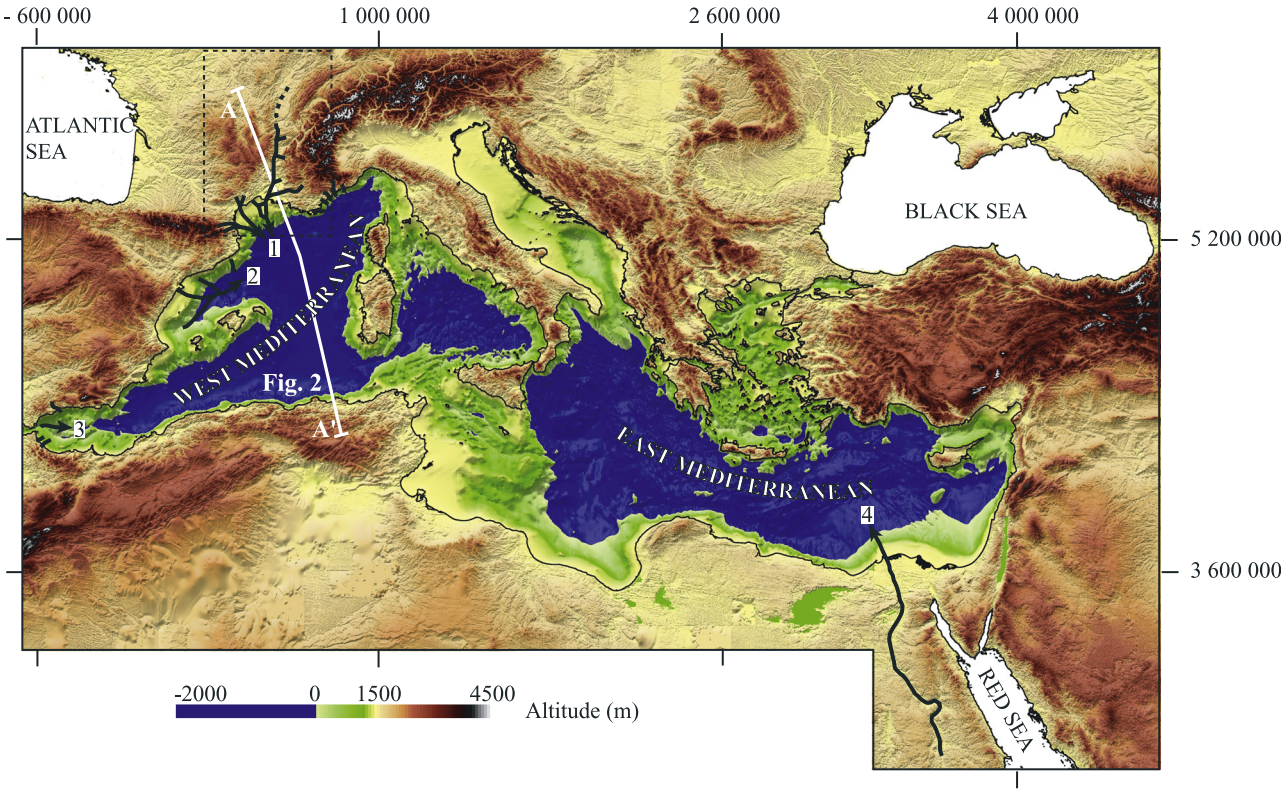

Figure 1. Digital elevation model of the Mediterranean region during the Messinian salinity crisis (GTOPO30 and ETOPO2, Mercator projection in meters). The thin black line shows the present shoreline. The blue areas are bounded by the −1500 m isobath as an estimate of the extent of Messinian sea level. Main Messinian drainage systems are shown (thick black lines): 1, Rhone-Pyrenean-Languedocian-Ligure [e.g., *Clauzon et al.*, 1995; *Guennoc et al.*, 2000]; 2, Valencia-Ebro [*Field and Gardner*, 1991; *Escutia and Maldonado*, 1992]; 3, Alboran [*Campillo et al.*, 1992; *Schoorl and Veldkamp*, 2003; *Loget et al.*, 2005]; 4, Nile [*Chumakov*, 1973; *Barber*, 1981]. The modeled domain in this study is shown by the dashed area. White line labeled A-A′ shows section in Figure 2.

the longitudinal profile of the Messinian Rhone to be restored (Figure 4). Previous work has emphasized the convex-up shape of the downstream part of this profile, which has been interpreted as resulting from a strong disequilibrium [*Clauzon*, 1982] compared to a "classical" graded profile. Remnants of pre-Messinian surfaces are present all along the current valley of the Rhone [*Clauzon*, 1982], enabling determination of the vertical incision that occurred during the MSC (Figure 5).

[16] Because the currently observable Messinian profile may have been affected by some post-Messinian tectonic deformation [*Steckler and Watts*, 1980; *Schlupp et al.*, 2001], we will use the vertical incision recorded along the profile rather that the shape of the profile itself, to compare the results of the numerical modeling with the geological data. This allows post-Messinian tectonics or general subsidence to be overlooked and we refer hereafter to the

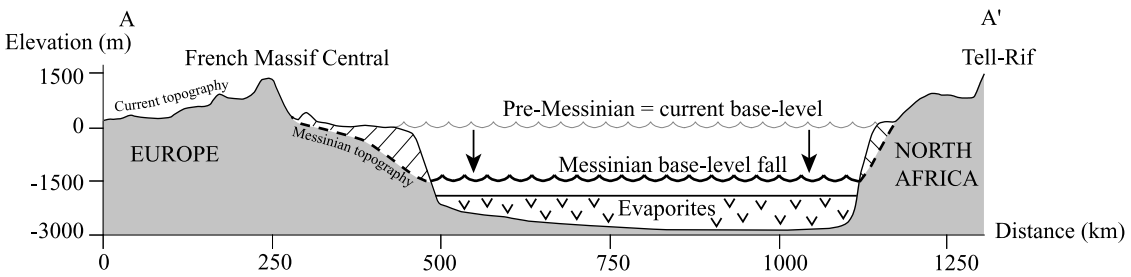

Figure 2. Schematic cross section in western Mediterranean showing the superimposed Messinian and current topography with their respective base levels (for location see Figure 1).

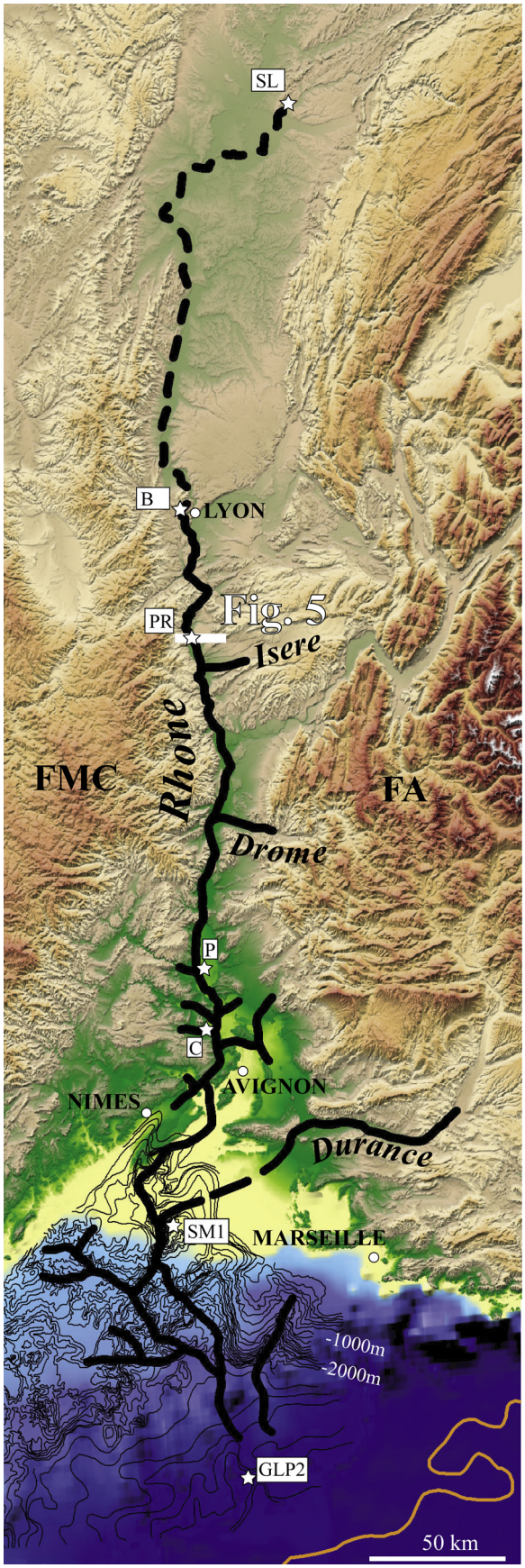

variation of the vertical incision along the Messinian Rhone profile as the cumulative erosion curve (Figure 6).

[17] We use the data published by *Clauzon* [1979, 1982], *Mandier* [1988], *Clauzon et al.* [1995], *Guennoc et al.* [2000], and *Baumard* [2001] to determine the vertical incision onshore and offshore (Table 1 and Figure 6). The lowest Mediterranean shoreline during the MSC is considered to match the limits of the Messinian evaporites [*Rouchy and Saint Martin*, 1992]. In the downstream part of the Rhone canyon, incision is not perceptible below the −2500 m Messinian isobath [*Guennoc et al.*, 2000]; we consider this boundary to be the limit for subaerial erosion. The upstream limit of Messinian incision has not been clearly identified in the Rhone Valley. Near Lyon, the vertical incision is around 300 m, so the upstream limit is certainly located farther upstream, possibly up to St Jean de Losne (in Bresse), about 200 km north of Lyon [*Baumard*, 2001] (Figures 3 and 4).

5. Modeling Procedure

[18] The general idea of this paper is to discuss the simplest average erosion model that can be compared with Messinian erosion. Unlike the approach developed by *Tomkin et al.* [2003] or *van der Beek and Bishop* [2003] which tested several models with the aim of validating a numerical model [e.g., *Oreskes et al.*, 1994], we have tested a single model in order to assess how the Messinian example constrains large-scale parameters such drainage area or slope, which are potentially accessible through geological archives.

[19] For this, we use a number of simplifications compatible with this objective of finding an average erosion model, with the geological knowledge described above, but also with the lack of knowledge intrinsic to such a large geological system.

[20] The first assumption is about the pre-Messinian topography. Analysis of the sediment record in the west Alpine foreland, including the Rhone Valley, shows that the direction of clastic supply during the Tortonian (upper Miocene) was similar to the present-day one, arguing for similar regional slopes as well [e.g., *Sissingh*, 2001; *Séranne et al.*, 2002]. In particular, according to *Mandier* [1988], remnants of alluvial deposits all along the Rhone Valley show that a paleo-Rhone was flowing into the Mediterranean before the MSC. Moreover, by looking at the length of preserved Messinian canyons around the Mediterranean, *Loget et al.* [2005] have argued that most Messinian drainage basins were similar in size to the present ones. Therefore the pre-MSC topography has been derived

Figure 3. Digital elevation model of southern France showing the Messinian drainage pattern (thick black lines). FMC, French Massif Central; FA, French Alps. Stars, boreholes where Messinian erosional surface is identified (SL, Saint Jean de Losne; B, Belle Allemande; PR, Peage du Roussilon; P, Pierrelate; C, Codolet; SM1, Saintes Marie); black solid lines, contour lines of the Messinian surface [after *Guennoc et al.*, 2000]; brown solid line, limit of the Messinian evaporites (lowest Messinian shoreline).

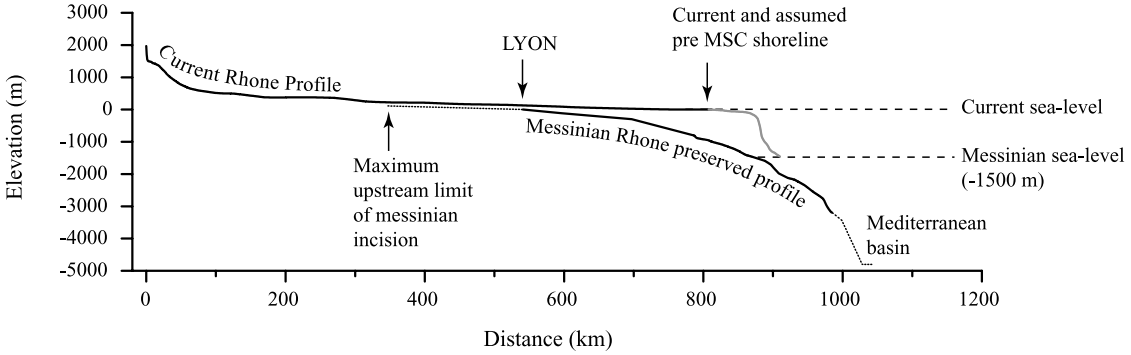

Figure 4. Present-day and Messinian profiles in the Rhone Valley and their respective base levels. Note the marked convex-up shape of the Messinian profile, indicating a state of strong disequilibrium.

from the GTOPO 30 DEM by resampling to a spatial resolution of 20 km. As our modeling approach is concerned with landscape evolution at regional scale, the resulting smoothed topography avoids the influence of local slopes (Figure 7). In order to mimic the Messinian sea level drop, the base level of the model has been fixed to the −1500 m current isobath, which roughly corresponds to the maximum present-day lateral extent of the Messinian evaporites [*Rouchy and Saint Martin*, 1992]. Moreover, according to *Gorini* [1993], the morphology of the Gulf of Lions shelf was most probably comparable to the present, including a similar location of the shelf break. Whether the sea level drop occurred in one or two steps, as suggested by *Clauzon et al.* [1996], is still debated. Hereafter we adopt the simplest scheme, i.e., one-step, instantaneous sea level fall.

[21] The second assumption concerns the erosion law. The law described in equation (1) is a mesoscale formulation, in the sense that it expresses the dependency of erosion and deposition fluxes with respect to some physical parameters that integrate local-scale complexity. The two parameters in equation (1) are local slope and water discharge. Local slope is defined at the resolution scale of calculation, which is about 4 km. Water discharge encompasses the flow variability within a river cross section. The validity of the mesoscale approach is intimately related to the choice of the mesoscale parameters. For the erosion equation, the main discussion is about the use of water discharge as a proxy for shear stress over the river bed. This is partially justified by phenomenological and heuristic relationships [*Howard et al.*, 1994; *Whipple and Tucker*, 1999], but the reader has to be aware that the discussion is far from closed even if most, if not all, landscape evolution models are built on this assumption.

[22] In this paper, we also assume that the erosion parameters (K, m, n, and ξ) are homogeneous over the entire system, in a way consistent with the search for an average fitting model. We could have considered two main departures from this homogeneous assumption: an erosion law that changes for small drainage area (according to the hillslope/channel dichotomy) or for large slopes (to include mass wasting processes), and a dependency with lithology. In the Messinian example, most, if not all, of the erosion is concentrated in the fluvial system. The steepness of the Messinian valley flanks [e.g., *Clauzon et al.*, 1995; *Schlupp et al.*, 2001] shows that both incision and the subsequent filling by Pliocene sediments have been too fast for hillslopes to respond significantly. On the other hand, the upstream migration of Messinian incision all around the Mediterranean appears to be controlled by the size of the upstream catchments whatever the variable nature of basement lithology in Mediterranean catchments [*Loget et al.*, 2005]. In this case, lithology does not appear to be a first-order parameter.

6. Results

[23] All runs were tested using the initial topography described above and with varying m, n, and ξ parameters (see Appendix B for equations parameters). Each model curve represents the variation in space of the amount of incision for a given period of time (represented by a dimensionless numerical time that depends on the average rainfall rate and on erodibility). Negative values of cumulative erosion mean that the model river aggrades. Experiment runs are stopped when experimental curves correspond to the global shape of the geological cumulative erosion curve, or when significant parameters, such as

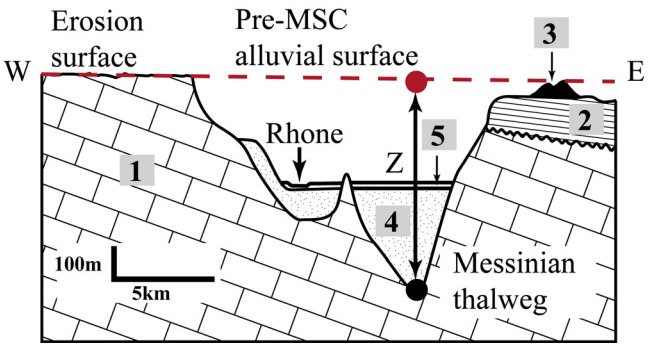

Figure 5. Method for determining vertical incision in the Rhone Valley during MSC [modified after *Clauzon*, 1982]. (see location in Figure 3). 1, Mesozoic; 2, Miocene; 3, remnants of pre-MSC alluvial surface; 4, Pliocene fill; 5, Quaternary alluvial deposits; Z, calculated incision.

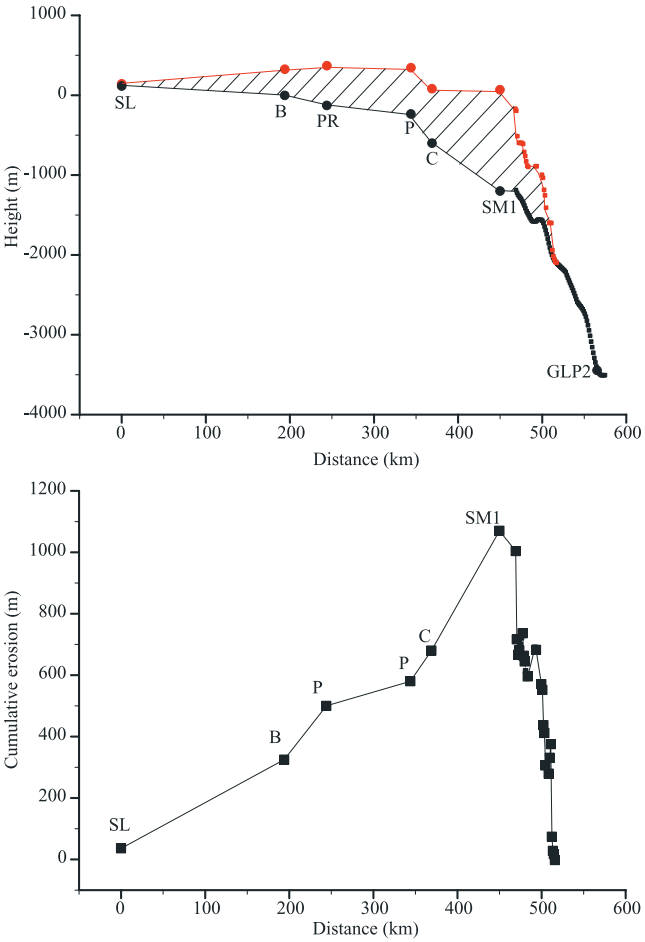

Figure 6. Vertical incision along the Messinian Rhone Valley. (top) Reconstruction of Messinian (black) and pre-MSC profiles (red) [data after *Clauzon*, 1982; *Guennoc et al.*, 2000; *Baumard*, 2001]. Circles, bore holes; square, seismic data; hatched area, amount of material removed (see Table 1). (bottom) Calculated cumulative erosion curve.

maximum amount of incision or headwater position are similar in both the experiment and nature. We also compare the 2D drainage pattern obtained in the experiments with that of the natural system.

6.1. Effect of m and n Parameters on the Incision Dynamics

[24] We first investigate the effects of m and n on the incision pattern in the Rhone Valley and for a fixed ξ value, which is smaller than the grid size (actually 4 km) (Figure 8).When $n = 1$, an increase of m favors erosion at large drainage areas according to equation (1). In a general way the model time required to reach the peak of erosion decreases when m increases.

[25] For $n = 1$ and $m = 1$ (the linear case), sedimentation occurs in the upstream part of the drainage area from the early stages onward ($t = 2500$) whereas erosion is distributed in the downstream part. At $t = 50{,}000$, only the downstream part of the model curve is correlated with the observed geological one. The 2D drainage pattern does not display localized narrow incision in the Rhone Valley or its tributaries.

[26] For $n = 1$ and $m = 2$, the peak of erosion is reached after a very short numerical time ($t = 0.15$). Propagation of incision up to the headwater position requires additional time ($t = 0.4$), but involves erosion exceeding that observed, in particular between 200 km and 400 km. In 2D view, a narrowly incised canyon occurs within the Rhone Valley but tributaries are weakly developed.

[27] For $n = 1$ and $m = 1.5$, the experimental curves fit rather well with the geological data curve for $20 < t < 40$. The 2D experimental pattern also resembles the natural system, characterized by the presence of a major canyon in the Rhone Valley and of several well-developed tributaries.

[28] Increasing the value of n favors erosion along the steepest slopes and reduces the influence of the drainage area, according to equation (1), especially for $m > 1$. In a general way, an increase of n, for a fixed value of m, raises the upstream propagation rate of incision.

[29] For $n = 2$ and $m = 1$, fluvial incision is restricted to the very downstream part of the drainage area, where the slopes are highest, whereas sedimentation occurs in the upstream part. The experiment was stopped at $t = 1250$ and much more additional time would be required to reach both the upstream limit of incision and the peak of erosion, whereas at $t = 500$ the landscape is still very smooth.

[30] For $n = 2$ and $m = 1.5$, the downstream part of the profile fits rather well with the geological profile at $t = 50$, but sedimentation tends to develop while approaching the headwaters. Moreover the 2D view shows that erosion is achieved through a denser drainage network with much broader valleys than in the natural system.

[31] For $n = 2$ and $m = 2$, the upstream limit of incision is reached at $0.375 < t < 0.5$, but with an amount of erosion in excess of that observed for geological data. In 2D view, although the drainage pattern as a whole resembles the

Table 1. Vertical Messinian Incision Along the Rhone Valley Deduced From Geological Data[a]

Boreholes	Distance From Upstream, km	Altitude of Pre-MSC Surface, m	Altitude of MSC Thalweg, m	Incision, m	Source
GLP2	565	−3437	−3437	0	*Guennoc et al.* [2000]
SM1 and seismic data	450	−114	−1200	1086	*Clauzon* [1979], *Guennoc et al.* [2000]
Codolet	369	erased	−650	700[b]	*Baumard* [2001]
Pierrelate	344	+340	−236	580	*Clauzon* [1982]
Péage du Roussillon	244	+360	−130	490	*Clauzon* [1982], *Clauzon et al.* [1995]
Belle Allemande	194	+300	0	300	*Baumard* [2001], *Mandier* [1988]
St Jean de Losne	0	erased	+114	10[b]	*Baumard* [2001]

[a]See borehole location on Figure 6.
[b]Minimum estimate determined from the present-day erosion surface, the pre-MSC surface being removed.

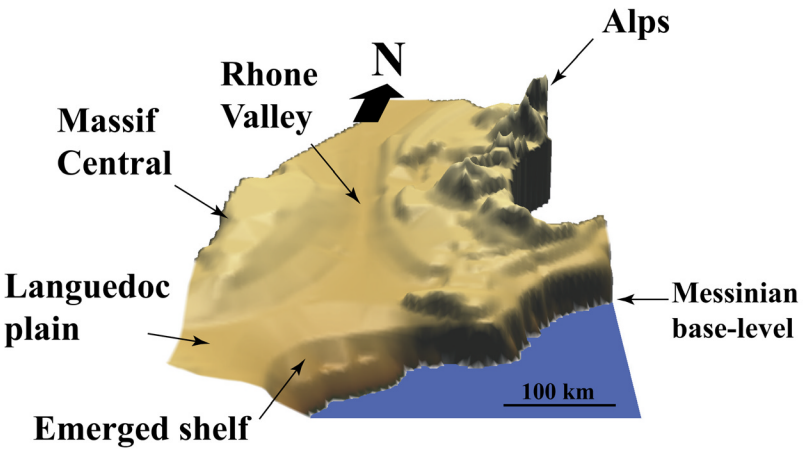

Figure 7. Initial topography used in the modeling. The topography is obtained by smoothing the present-day topography to a spatial resolution of 20 km per pixel and by fixing the sea level to the present-day −1500 m isobath (vertical exaggeration 32 times).

natural system, incision has propagated too far inland, in regard to the tributaries.

[32] In conclusion, for a small transport length ($\xi \leq 4$ km), the best fit between the geological data and the model results is obtained for an exponent combination of $m = 1.5$ and $n = 1$.

6.2. Effect of the ξ Parameter on the Incision Dynamics

[33] An increase of the transport length makes the river behavior evolve from an advective/diffusive-like model for low ξ (in the sense that the topographic evolution intrinsically contains an "advective"-like term that depends on slope, plus a "diffusive"-like term that depends on curvature) toward a complete evacuation of the erosion products for large ξ [*Crave and Davy*, 2001]. In the numerical experiments, the larger the value of ξ, the faster the propagation of erosion.

[34] Hereafter, we focus on the effect of the transport length for two exponent combinations: $m = 1.5$ and $n = 1$, and $m = 1$ and $n = 1$ respectively. The second combination is the linear case that corresponds to a surrogate of the "undercapacity model" commonly used in other numerical simulations [e.g., *Kooi and Beaumont*, 1994].

[35] For $m = 1.5$ and $n = 1$, an increase of ξ from a value less than 4 km up to 400 km moves the experimental curve away from the geological data (Figure 9). For ξ = 40 km, both curves still show a similar overall geometry during the first stages in the downstream part, but much more erosion is needed to reach the upstream limit of incision than in the natural system. For ξ = 400 km, the experimental curves cut across the geological curve as soon as the experiment starts and their shape never matches the geological curve. Reaching the headwater would require a considerable amount of erosion. In 2D, an increase of ξ inhibits the development of tributaries and erosion is concentrated within one major canyon.

[36] In the linear case ($m = 1$, $n = 1$), both the experimental curves and the 2D views (Figure 10) show that an increase of ξ helps incision to propagate upstream but does not allow a good fit with the geological data. As in the previous case ($m = 1.5$, $n = 1$), a large ξ (400 km) needs much more erosion to reach the upstream limit of incision.

[37] In conclusion, testing the influence of the transport length reinforces the relevance of the exponent combination deduced from the first set of experiments, namely $m = 1.5$, $n = 1$ and $\xi \leq 4$ km.

6.3. Evolution With Time of the Drainage for m = 1.5, n = 1, and ξ ≤ 4 km

[38] Figure 11 shows successive stages of the network growth during an experimental run for $m = 1.5$, $n = 1$ and $\xi \leq 4$ km. Incision first develops on the edge of the emerged topography inside the Rhone Valley ($t = 1$). At $t = 10$, two major canyons have propagated far inland (in the Rhone Valley and the Languedoc plain). At $t = 40$, incision of tributaries that initiated during the previous stages, extends inland, whereas the major canyons continue to propagate inland. Concerning erosion dynamics in the Rhone Valley, the experimental curves show that incision develops very fast during the early stages in the downstream part (from $t = 0$ to $t = 5$). The upstream limit of incision (ULi) propagates about 350 km inland, whereas the peak of erosion, whose value reaches 650 m (Epy), is located only 70 km from the outlet (Epx). In further stages, (from $t = 5$ to $t = 40$), the headwater migration slows down whereas the peak of erosion rises to 1100 m. The time interval that best accounts for the geological data is from $t = 20$ to $t = 40$. This evolution as a whole corresponds to a diffusive relaxation of the river longitudinal profile with time (Figure 11c). This also results in a nonlinear behavior of sedimentation in the downstream basin, the bulk of the discharge being evacuated during the first stages (Figure 12).

7. Discussion

[39] The first set of experiments shows that a necessary condition to reproduce the Messinian erosion pattern in the Rhone Valley using the ϵros model formulation is $m > 1$ and $m > n$, emphasizing the crucial role of the drainage area in the propagation of the erosion. Experimental results

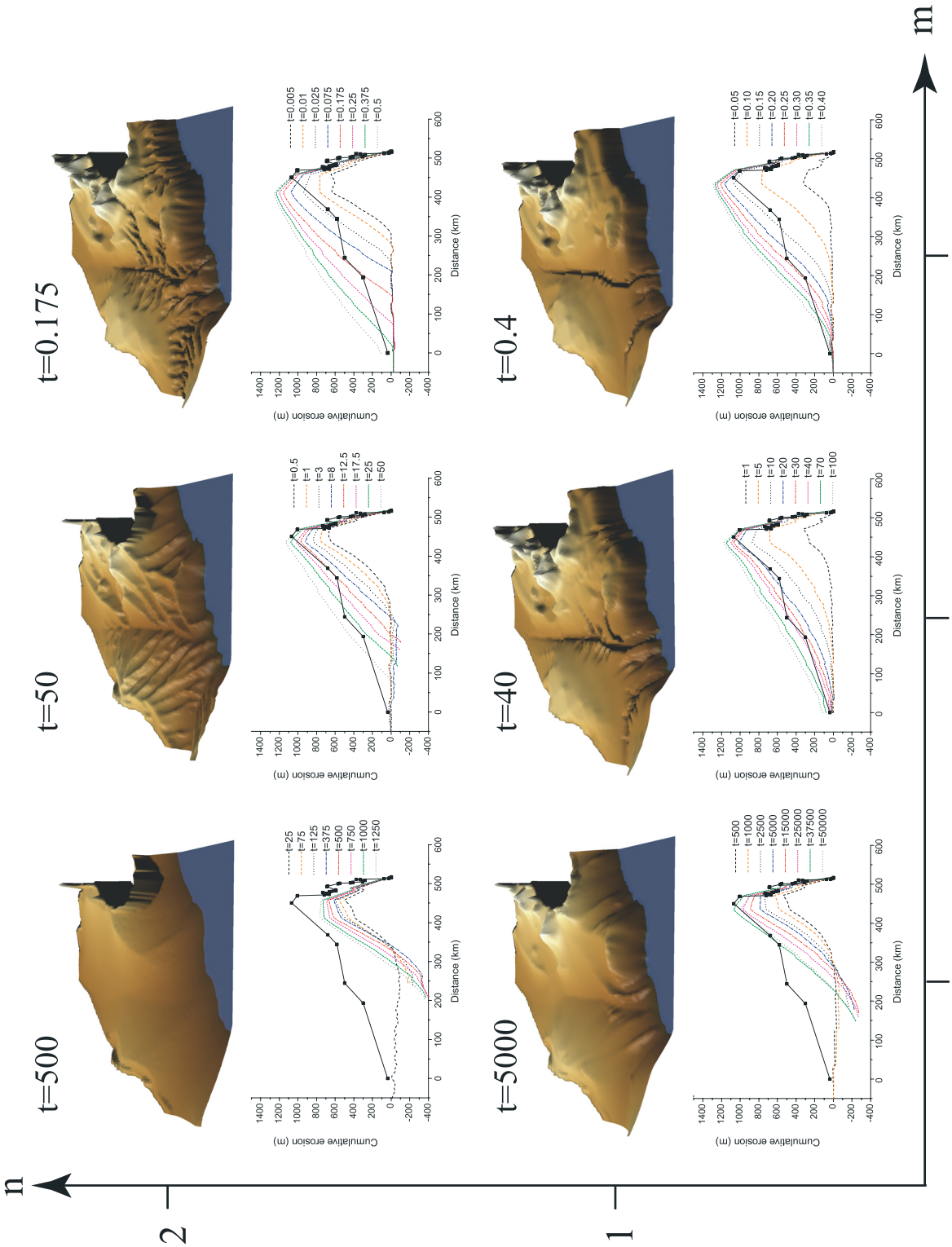

Figure 8. Numerical modeling showing the effect of m and n variations on Messinian erosion pattern for $\xi < 4$ km (pixel size of 4 km). Top plots: 2-D view of the models (vertical exaggeration 32 times). Bottom plots: experimental cumulative erosion curves at different times (colored lines) and geological data (black line). Best fit between numerical results and geological data is obtained for $m = 1.5$ and $n = 1$.

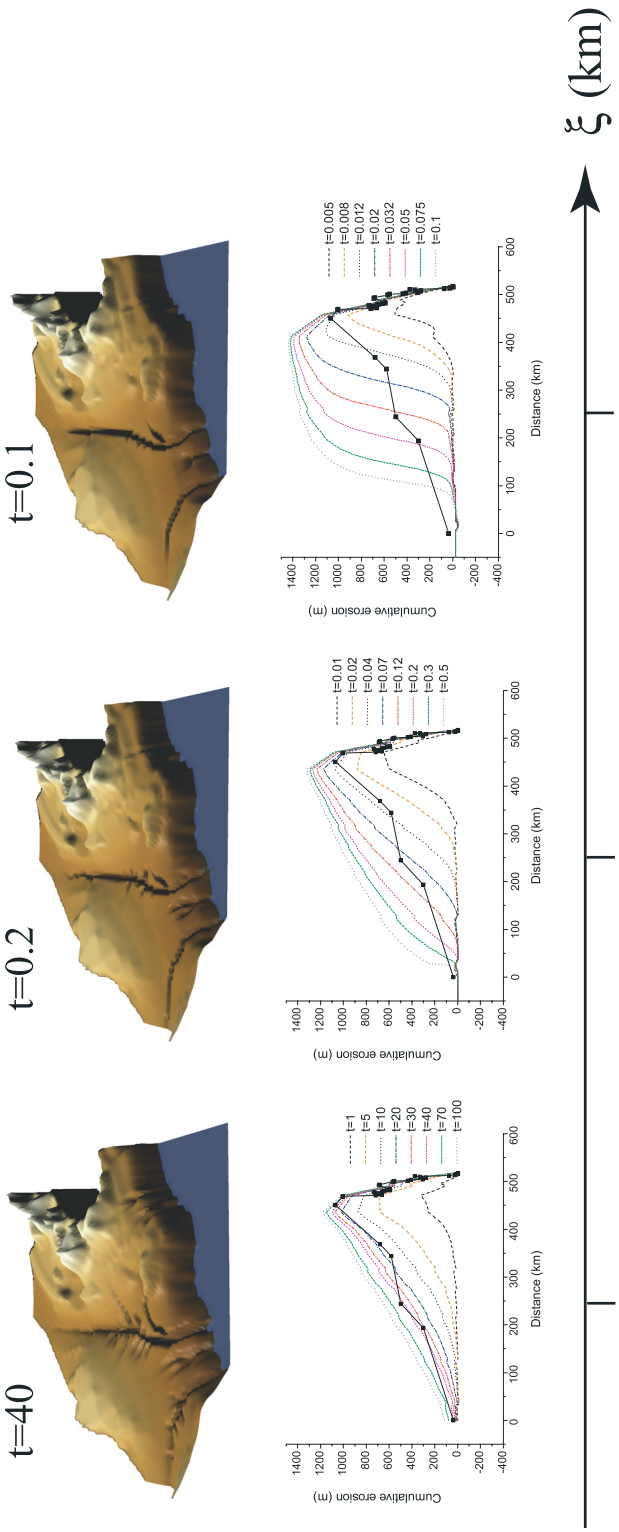

Figure 9. Numerical modeling showing the effect of an increasing transport length (ξ) on Messinian erosion pattern for $m = 1.5$ and $n = 1$. Top plots: 2-D view of the models (vertical exaggeration 32 times). Bottom plots: experimental cumulative erosion curves at different times (colored lines) and geological data (black line).

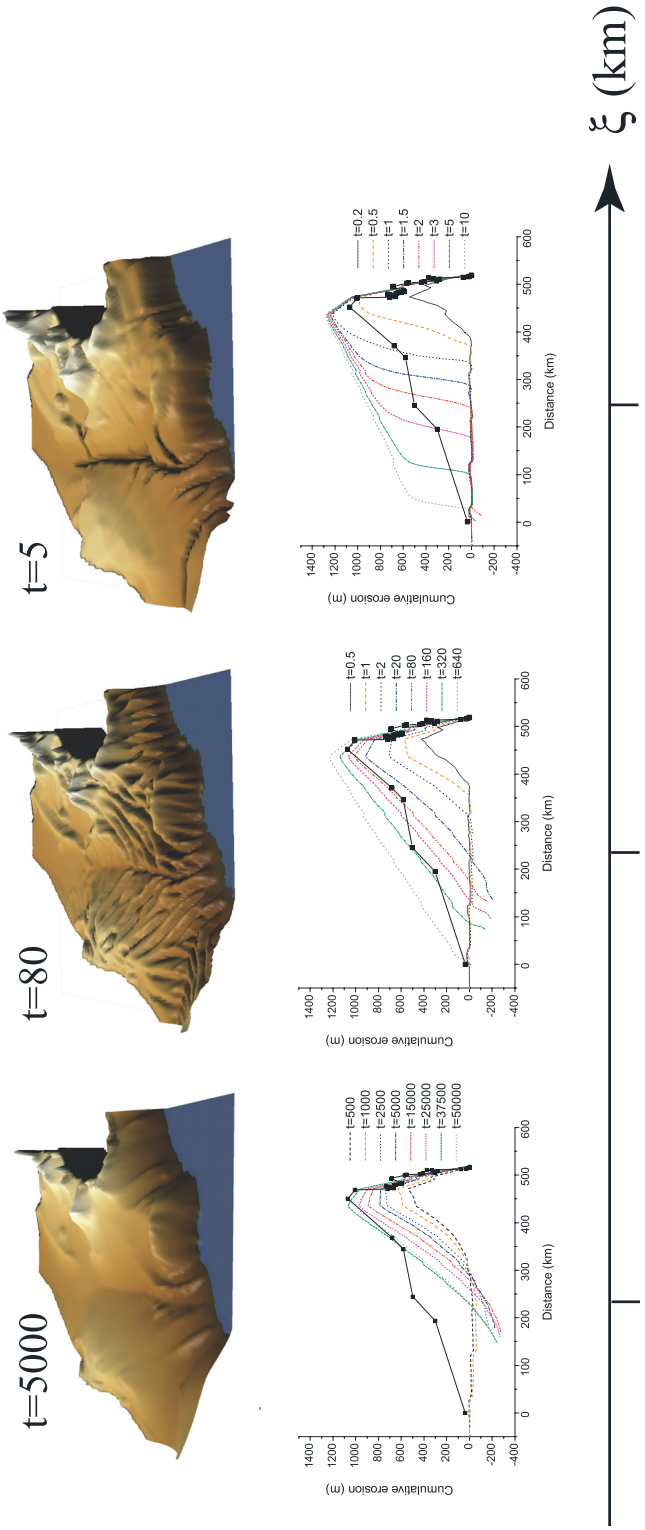

Figure 10. Numerical modeling showing the effect of an increasing transport length (ξ) on Messinian erosion pattern for $m = 1$ and $n = 1$ (linear case). Top plots: 2-D view of the models (vertical exaggeration 32 times). Bottom plots: experimental cumulative erosion curves at different times (colored lines) and geological data (black line).

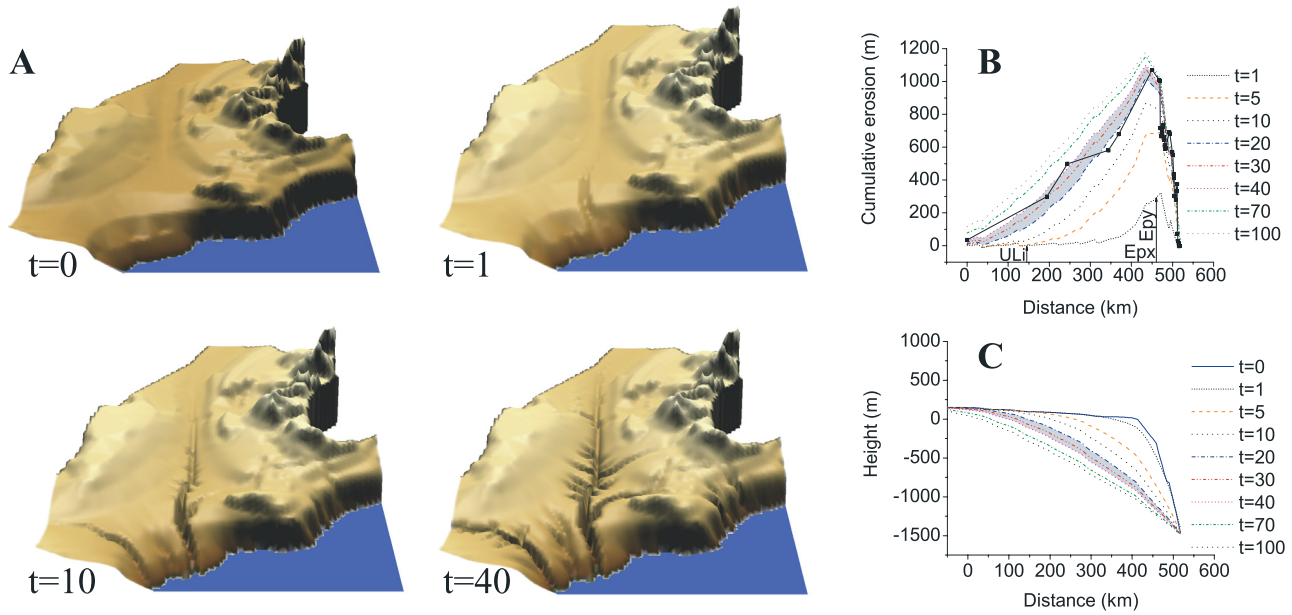

Figure 11. Run of a numerical experiment using the best combination of parameters (m = 1.5, n = 1, ξ < 4 km). (a) Two-dimensional views. (b) Experimental curve at different times (colored lines) compared to the geological curve (black line). (c) Evolution of the longitudinal profile with time. The best fitting model time interval (t = 20 to t = 40) is deduced from agreement with geological data (gray area). ULi, upstream limit of incision; Epy, peak of vertical incision; Epx, position of the peak of vertical incision.

provide values of m and n of 1.5 and 1 respectively. These values are similar to those described in previous studies that assumed a transport limited case [*Murray and Paola*, 1997; *Crave and Davy*, 2001; *Whipple and Tucker*, 2002; *Lague and Davy*, 2003; *Clevis et al.*, 2004]. These values also provide a concavity index of 0.5 (defined as $\theta' = m' - 1/n'$, in the transport limited case). Similar values ($0.4 < \theta < 0.7$) have been reported from natural drainage systems [e.g., *Hack*, 1957; *Tarboton et al.*, 1989; *Massong and Montgomery*, 2000]. As an example, the current Rhone basin provides a comparable value of around 0.4 (Figure 13).

[40] The second set of experiments shows that propagating the incision far inland, while confining most of the erosion to the downstream valley, requires a small transport length ξ, i.e., smaller than a couple of kilometers.

[41] A decrease of the transport length tends to erase the initial break in slope. In the experiments the largest (ξ = 400 km) and the smallest (ξ < 4 km) transport lengths constitute two end-member modes of this knickpoint evolution, namely "parallel knickpoint retreat" or "knickpoint replacement" respectively (Figure 14) [e.g., *Gardner*, 1983].

[42] A small transport length implies a transport-limited mode of fluvial erosion [e.g., *Kooi and Beaumont*, 1994]. In the present case, the transport length is at least two orders of magnitude smaller than the length scale of the drainage system. This suggests that the response of the drainage system, subsequent to the Messinian base level drop, was transport-limited, implying the diffusive-like evolution of the Rhone profile and the progressive replacement of the initial break in slope.

[43] The migration of knickpoints is usually interpreted as corresponding to transient stages in the evolution of river profiles toward equilibrium (graded profile). Conversely, the absence of knickpoints is considered to be symptomatic of a profile close to equilibrium, except equilibrium knickpoints that are due to lithological variation or due to spatially variable tectonic uplift rates. Although knickpoints

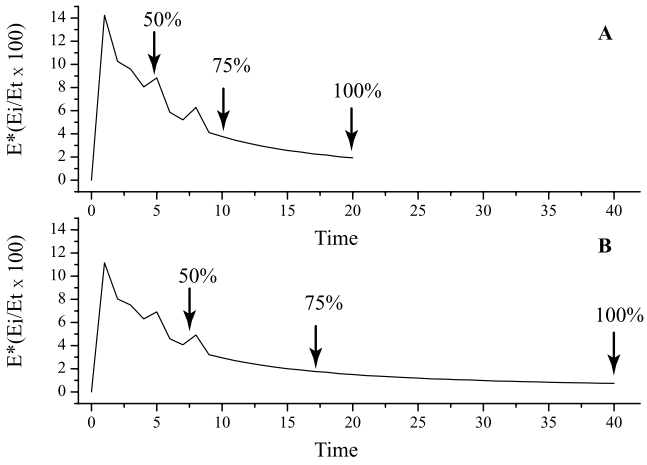

Figure 12. Variation of the amount of removed material in the modeled Rhone Valley. The amount of erosion between two time steps (E_i) is normalized by the total erosion (E_t). The fraction of total erosion (E*) is indicated in percent. (a) Percentage of sediments removed at a given time for the first numerical time interval confidence t = 20. (b) Percentage of sediments removed at a given time for the second numerical time interval confidence t = 40. Note that most of sediment is evacuated in early stages in both cases, i.e., 50% of the total eroded material is evacuated at t = 5 for the experiment stopped at t = 20 (Figure 12a) and at t = 7.5 for the experiment stopped at t = 40 (Figure 12b).

do not occur along the Messinian Rhone profile, its convex-up shape due to a very large knick zone [*Zaprowski et al.*, 2001] shows that has not reached equilibrium. In addition, owing to the short duration of the Messinian sea level drop (10^5 years), the preserved Messinian Rhone profile can be considered as corresponding to a transient stage of an aborted river response to a base level drop.

[44] A similar river response of incision far inland from the river mouth (10 s to 100 s km) without clear evidence of knickpoint propagation, has been reported from the study of Quaternary eustatic variations on comparable timescales, but for amplitudes of hundreds, rather than thousands, of meters [e.g., *Blum and Törnqvist*, 2000; *Van Heijst and Postma*, 2001]. So, this tends to show that it is not so much the amplitude of the base level fall that is relevant to account for the rate of inland incision but rather the size of the upstream catchments [*Loget et al.*, 2005].

8. Conclusion

[45] The modeling of the Messinian Rhone Valley provides new insights into the understanding of the migration of incision subsequent to a major base level drop. First, the values obtained for the exponents m and n of the fluvial incision law are in agreement with those obtained from the analysis of natural systems and from previous experimental studies. The drainage area and the sediment transport length in rivers are two predominant parameters during the response of a drainage network to the fall of its base level. Concentration and propagation of incision require a nonlinear exponent m (m = 1.5) on drainage area as a proxy for water discharge. A very low value of ξ ($\leq$4 km) makes it possible for incision to propagate very far inland (up to 500 km) without knickpoint migration. Such behavior may be considered as a diffusive process at large length scale. This was already suspected in the case of the response to Quaternary eustatic variations whose vertical amplitude does not exceed some tens of m on a similar time duration as the Messinian salinity crisis. Finally, propagation of fluvial incision appears to be very fast at geological timescales, but restoration of an equilibrium profile is a very long term process because of the diffusive-like behavior response of rivers after a base level fall.

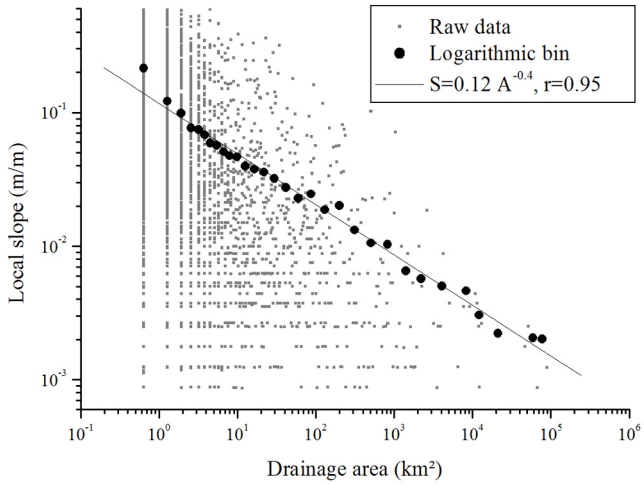

Figure 13. Area-slope relationship for the present-day drainage basin of the Rhone River, derived from digital topographic data with resolution of 200 m.

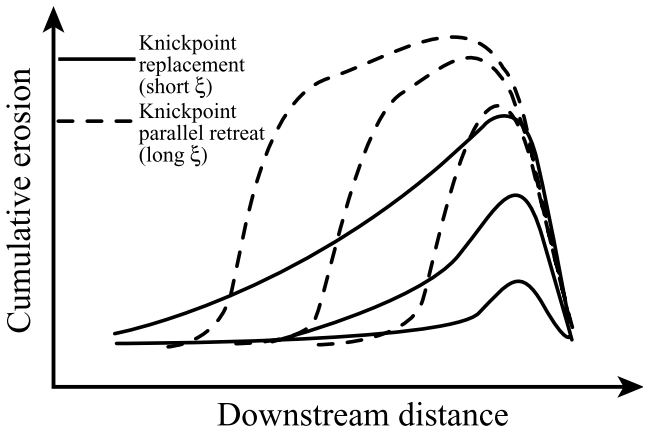

Figure 14. Significance of the shape of the cumulative erosion curve with regard to large and small values of ξ respectively.

Appendix A: End-Member Models

[46] To demonstrate how the constitutive equations behave for both end-member models of $\xi \ll 1$ and $\xi \gg 1$, we calculate the solution on a pixel $[x, x + dx]$ where $\dot{e}$ is assumed constant. By integrating the equation between x and $x + dx$, we obtain

$$dS = S(x+dx) - S(x) = \left(\frac{\xi\dot{e}}{v} - S(x)\right)\left(1 - e^{\frac{-dx}{\xi}}\right)$$

If ξ is very large, the last term of the previous equation simplifies such as

$$dh = -dS \approx -\left(\frac{\xi\dot{e}}{v} - S(x)\right)\frac{dx}{\xi} \approx -\dot{e}\frac{dx}{v} = -\dot{e}dt$$

The equivalent equation is thus

$$\frac{\partial h}{\partial t} = -\dot{e}$$

If now ξ is very small compared to dx, the equation becomes

$$S(x+dx) = \frac{\xi\dot{e}}{v}$$

which means that the river load is in equilibrium with the erosion rate at the end of the pixel. Accordingly the river load $S(x)$ at the entry of the pixel is given by the erosion of the previous pixel, and the difference can be expressed as

$$dh = S(x) - S(x+dx) = \left[\frac{\xi\dot{e}}{v}\right]_{x-dx} - \left[\frac{\xi\dot{e}}{v}\right]_{x} \approx -\frac{\partial}{\partial x}(\xi\dot{e})\frac{dx}{v} = -\frac{\partial}{\partial x}(\xi\dot{e})dt$$

The equivalent derivative equation is $\frac{\partial h}{\partial t} = -\vec{\nabla}(\xi \dot{e}\vec{n})$, where $\vec{n}$ is the flow direction.

Appendix B: Equation Parameters

[47] The process variables are

r the rainfall rate;
(K, m, n, ξ) the coefficients of the erosion/deposition law;
Δx the grid cell length (4 km);
a_o the cell area (4×4 km^2);
h_o the vertical unit (1 m).

For the calculations, we define the following characteristic variables: the characteristic discharge $Q_o = ra_o$ and the characteristic slope s_o, which is given by the ratio between vertical and horizontal units: $s_o = \frac{h_o}{\Delta x_o}$. The characteristic timescale is $t_o = \frac{h_o}{\dot{e}(Q_o, s_o)}$, which derives from the constitutive equation. $\dot{e}(Q_o, s_o)$ is the erosion rate for the characteristic discharge and slope.

[49] The dynamic equation is calculated with dimensionless variable

$$h^* = h/h_o$$

$$x^* = x/\Delta x$$

$$s^* = s/s_o$$

$$Q^* = Q/Q_o$$

$$t^* = t/t_o$$

The dimensionless erosion law is

$$\dot{e}(Q^*, s^*) = Q^{*m} s^{*n}$$

$$\xi^* = \xi/\Delta x$$

[50] **Acknowledgments.** We are grateful to Peter van der Beek, Philip Allen, and an anonymous referee for thorough and constructive reviews. We also thank Julien Babault, Dimitri Lague, and Sébastien Castelltort for helpful discussions at various stages of this work. Financial support was provided by Centre National de la Recherche Scientifique INSU, "Programme Relief de la Terre," and by the Ministère de l'Education, de la Recherche et de la Technologie, who funded Nicolas Loget's Ph.D.

References

Ballesio, R. (1972), *Etude stratigraphique du Pliocène rhodanien, Doc. Lab. Géol. Fac. Sci. Lyon*, vol. 53, 333 pp., Univ. Claude Bernard Lyon 1, Lyon, France.

Barber, P. M. (1981), Messinian subaerial erosion of the Proto-Nile delta, *Mar. Geol.*, *44*, 253–272.

Baumard, B. (2001), Valorisation de données pour l'étude de la crise messinienne dans le Gard rhodanien et la moitié est de la France, Ph.D. thesis, 260 pp., Ecole des Mines de Paris, Paris.

Beaumont, C., P. Fullsack, and J. Hamilton (1992), Erosional control of active compressional orogens, in *Thrust Tectonics*, edited by K. R. McClay, pp. 1–18, CRC Press, Boca Raton, Fla.

Blanc, P. L. (2002), The opening of the Plio-Quaternary Gibraltar Strait: Assessing the size of a cataclysm, *Geodin. Acta*, *15*, 303–317.

Blum, M. D., and T. E. Törnqvist (2000), Fluvial responses to climate and sea-level change: A review and look forward, *Sedimentology*, *47*, 2–48.

Braun, J., and M. Sambridge (1997), Modelling landscape evolution on geological time scales: A new method based on irregular spatial discretization, *Basin Res.*, *9*, 27–52.

Burbank, D. W., J. Leland, E. Fielding, R. S. Anderson, N. Brozovic, M. R. Reid, and C. Duncan (1996), Bedrock incision, rock uplift and threshold hillslopes in the northwestern Himalayas, *Nature*, *379*, 505–510.

Campillo, A., A. Maldonado, and A. Mauffret (1992), Stratigraphic and tectonic evolution of the western Alboran sea: Late Miocene to recent, *Geo Mar. Lett.*, *12*, 165–172.

Chase, C. G. (1992), Fluvial landsculpting and the fractal dimension of topography, *Geomorphology*, *5*, 39–57.

Chumakov, I. S. (1973), Pliocene and Pleistocene deposits of the Nile valley in Nubia and upper Egypt, *Initial Rep. Deep Sea Drill. Proj.*, *13*, 1242–1243.

Clauzon, G. (1978), The Messinian Var canyon (Provence, southern France): Paleogeographic implications, *Mar. Geol.*, *27*, 231–246.

Clauzon, G. (1979), Le canyon messinien de la Durance (Provence, France): Une preuve paléogéographique du bassin profond de dessication, *Palaeogeogr. Palaeoclimatol. Palaeoecol.*, *29*, 15–40.

Clauzon, G. (1982), Le canyon messinien du Rhône: Une preuve décisive du "dessicated deep basin model" (Hsü, Cita et Ryan, 1973), *Bull. Soc. Geol. Fr.*, *24*, 231–246.

Clauzon, G., J. L. Rubino, and B. Savoye (1995), Marine Pliocene Gilbert-type fan deltas along the French Mediterranean coast: A typical infill feature of preexisting subaerial Messinian canyons, in *16th IAS Regional Meeting of Sedimentology*, *Field Trip Guidebook*, vol. 23, pp. 143–222, Assoc. des Sedimentol. Fr., Paris.

Clauzon, G., J. P. Suc, F. Gautier, A. Berger, and M. F. Loutre (1996), Alternate interpretation of the Messinian salinity crisis: Controversy resolved?, *Geology*, *24*, 363–366.

Clevis, Q., P. L. De Boer, and W. Nijman (2004), Differentiating the effect of episodic tectonism and eustatic sea-level fluctuations in foreland basins filled by alluvial fans and axial deltaic systems: Insights from a three-dimensional stratigraphic forward model, *Sedimentology*, *51*, 809–835.

Crave, A., and P. Davy (2001), A stochastic "precipiton" model for simulating erosion/sedimentation dynamics, *Comput. Geosci.*, *27*, 815–827.

Davy, P., and A. Crave (2000), Upscaling local-scale transport processes in large-scale relief dynamics, *Phys. Chem. Earth, Part A*, *25*(6–7), 533–541.

Denizot, G. (1952), Le Pliocène dans la vallée du Rhône, *Rev. Geogr. Lyon*, *27*, 327–357.

Escutia, C., and A. Maldonado (1992), Paleogeographic implications of the Messinian surface in the Valencia trough, northwestern Mediterranean Sea, *Tectonophysics*, *203*, 263–284.

Field, M. E., and J. V. Gardner (1991), Valencia gorge: Possible Messinian refill channel for the western Mediterranean Sea, *Geology*, *19*, 1129–1132.

Gardner, T. W. (1983), Experimental study of knickpoint and longitudinal profile evolution in cohesive, homogeneous material, *Geol. Soc. Am. Bull.*, *94*, 664–672.

Gorini, C. (1993), Géodynamique d'une marge passive: Le Golfe du Lion (Méditerranée occidentale), Ph.D. thesis, 264 pp., Univ. Paul Sabatier de Toulouse III, Toulouse, France.

Guennoc, P., C. Gorini, and A. Mauffret (2000), Histoire geologique du Golfe du Lion et cartographie du rift oligo-aquitanien et de la surface messinienne, *Geol. Fr.*, *3*, 67–97.

Hack, J. T. (1957), Studies of longitudinal stream profiles in Virginia and Maryland, *U. S. Geol. Surv. Prof. Pap.*, *294-B*, 97 pp.

Howard, A. D. (1994), A detachment-limited model of drainage basin evolution, *Water Resour. Res.*, *30*, 2261–2285.

Howard, A. D., W. E. Dietrich, and M. A. Seidl (1994), Modeling fluvial erosion on regional to continental scales, *J. Geophys. Res.*, *99*, 13,971–13,986.

Hsü, K. J., M. B. Cita, and W. B. F. Ryan (1973), The origin of the Mediterranean evaporates, *Initial Rep. Deep Sea Drill. Proj.*, *13*, 1203–1231.

Kooi, H., and C. Beaumont (1994), Escarpment evolution on high-elevation rifted margins: Insights derived from a surface processes model that combines diffusion, advection, and reaction, *J. Geophys. Res.*, *99*, 12,191–12,209.

Krijgsman, W., F. J. Hilgen, I. Raffi, F. J. Sierro, and D. S. Wilson (1999), Chronology, causes and progression of the Messinian salinity crisis, *Nature*, *400*, 652–655.

Lague, D., and P. Davy (2003), Constraints on the long-term colluvial erosion law by analyzing slope-area relationships at various tectonic uplift rates in the Siwaliks Hills (Nepal), *J. Geophys. Res.*, *108*(B2), 2129, doi:10.1029/2002JB001893.

Loget, N., J. Van Den Driessche, and P. Davy (2005), How did the Messinian salinity crisis end?, *Terra Nova*, *17*, 414–419.
Mandier, P. (1988), Le relief de la moyenne vallée du Rhône au Tertiaire et au Quaternaire: Essai de synthèse paléogéographique, *Doc. BRGM 151*, Bur. de Rech. Géol. et Min., Orleans, France.
Martín, J. M., J. C. Braga, and C. Betzler (2001), The Messinian Guadalhorce corridor: The last northern, Atlantic-Mediterranean gateway, *Terra Nova*, *13*, 418–424.
Massong, T. M., and D. R. Montgomery (2000), Influence of sediment supply, lithology, and wood debris on the distribution of bedrock and alluvial channels, *Geol. Soc. Am. Bull.*, *112*, 591–599.
Murray, A. B., and C. Paola (1997), Properties of a cellular braided-stream model, *Earth Surf. Processes Landforms*, *22*, 1001–1025.
Oreskes, N., K. Shrader-Frechette, and K. Belitz (1994), Verification, validation, and confirmation of numerical models in the earth sciences, *Science*, *263*, 641–646.
Pinet, P., and M. Souriau (1988), Continental erosion and large-scale relief, *Tectonics*, *7*, 563–582.
Rouchy, J. M., and J. P. Saint Martin (1992), Late Miocene events in the Mediterranean as recorded by carbonate-evaporite relations, *Geology*, *20*, 629–632.
Ryan, W. B. F. (1976), Quantitative evaluation of the depth of the western Mediterranean before, during and after the late Miocene salinity crisis, *Sedimentology*, *23*, 791–813.
Schlupp, A., G. Clauzon, and J. P. Avouac (2001), Mouvement post-messinien sur la faille de Nîmes: Implications pour la sismotectonique de la Provence, *Bull. Soc. Geol. Fr.*, *172*, 697–711.
Schoorl, J. M., and A. Veldkamp (2003), Late Cenozoic landscape development and its tectonic implications for the Guadalhorce valley near Alora (southern Spain), *Geomorphology*, *50*, 43–57.
Séranne, M., H. Camus, F. Lucazeau, J. Barbarand, and Y. Quinif (2002), Surrection et érosion polyphasées de la bordure cévenole: Un exemple de morphogenèse lente, *Bull. Soc. Geol. Fr.*, *173*, 97–112.
Sissingh, W. (2001), Tectonostratigraphy of the West Alpine Foreland: Correlation of Tertiary sedimentary sequences, changes in eustatic sea-level and stress regimes, *Tectonophysics*, *333*, 361–400.
Snyder, N. P., K. X. Whipple, G. E. Tucker, and D. J. Merritts (2000), Landscape response to tectonic forcing: DEM analysis of stream profiles in the Mendocino triple junction region, northern California, *Geol. Soc. Am. Bull.*, *112*(8), 1250–1263.
Steckler, M. S., and A. B. Watts (1980), The Gulf of Lion: Subsidence of a young continental margin, *Nature*, *287*, 425–429.
Stock, J. D., and D. R. Montgomery (1999), Geologic constraints on bedrock river incision using the stream power law, *J. Geophys. Res.*, *104*, 4983–4993.
Tarboton, D. G., R. L. Bras, and I. Rodriguez-Iturbe (1989), Scaling and elevation in river networks, *Water Resour. Res.*, *25*(9), 2037–2051.
Tomkin, J. H., M. T. Brandon, F. J. Pazzaglia, J. R. Barbour, and S. D. Willett (2003), Quantitative testing of bedrock incision models for the Clearwater River, NW Washington State, *J. Geophys. Res.*, *108*(B6), 2308, doi:10.1029/2001JB000862.
Tucker, G., and R. Slingerland (1996), Predicting sediment flux from fold and thrust belts, *Basin Res.*, *8*, 329–349.
Tucker, G. E., and K. X. Whipple (2002), Topographic outcomes predicted by stream erosion models: Sensitivity analysis and intermodel comparison, *J. Geophys. Res.*, *107*(B9), 2179, doi:10.1029/2001JB000162.
Tucker, G. E., S. T. Lancaster, N. M. Gasparini, and R. L. Bras (2001), The channel-hillslope integrated landscape development model (CHILD), in *Landscape Erosion and Evolution Modeling*, edited by R. S. Harmon and W. W. Doe III, pp. 349–388, Springer, New York.
van der Beek, P., and P. Bishop (2003), Cenozoic river profile development in the Upper Lachlan catchment (SE Australia) as a test of quantitative fluvial incision models, *J. Geophys. Res.*, *108*(B6), 2309, doi:10.1029/2002JB002125.
Van Heijst, M. W. I. M., and G. Postma (2001), Fluvial response to sea-level changes: A quantitative analogue, experimental approach, *Basin Res.*, *13*, 269–292.
Weijermars, R. (1988), Neogene tectonics in the western Mediterranean may have caused the Messinian salinity crisis and an associated glacial event, *Tectonophysics*, *148*, 211–219.
Willett, S. D., R. Slingerland, and N. Hovius (2001), Uplift, shortening and steady state topography in active mountain belts, *Am. J. Sci.*, *301*, 455–485.
Willgoose, G. R., R. L. Bras, and I. Rodriguez-Iturbe (1991), Results from a new model of river basin evolution, *Earth Surf. Processes Landforms*, *16*, 237–254.
Whipple, K. X. (2001), Fluvial landscape response time: How plausible is steady state denudation?, *Am. J. Sci.*, *301*, 313–325.
Whipple, K. X., and G. E. Tucker (1999), Dynamics of the stream-power river incision model: Implications for height limits of mountain ranges, landscape response timescales, and research needs, *J. Geophys. Res.*, *104*(B8), 17,661–17,674.
Whipple, K. X., and G. E. Tucker (2002), Implications of sediment-flux-dependent river incision models for landscape evolution, *J. Geophys. Res.*, *107*(B2), 2039, doi:10.1029/2000JB000044.
Zaprowski, B. J., E. B. Evenson, F. J. Pazzaglia, and J. B. Epstein (2001), Knickzone propagation in the Black Hills and northern High Plains: A different perspective on the late Cenozoic exhumation of the Laramide Rocky Mountains, *Geology*, *29*, 547–550.

P. Davy, N. Loget, and J. Van Den Driessche, Géosciences Rennes, UMR 6118, CNRS, Université de Rennes 1, Rennes, France. (nicolas.loget@univ-lr.fr)